Evaporating Potential

Sunmiao Fang
Nanjing University of Aeronautics and Astronautics
Jidong Li
Nanjing University of Aeronautics and Astronautics
Yin Xu
Nanjing University of Aeronautics and Astronautics
Chun Shen
Nanjing University of Aeronautics and Astronautics
Wanlin Guo (wlguo@nuaa.edu.cn)
Nanjing University of Aeronautics and Astronautics https://orcid.org/0000-0002-2302-8044

Letter

Keywords: Functional Materials, Hydrovaltaics, Porous Carbon Black Film, Carrier Transfer

Posted Date: October 16th, 2020

DOI: https://doi.org/10.21203/rs.3.rs-86256/v1

Version of Record: A version of this preprint was published at Joule on March 1st, 2022. See the published version at https://doi.org/10.1016/j.joule.2022.02.002.

Evaporating Potential

Sunmiao Fang, Jidong Li, Ying Xu, Chun Shen, Wanlin Guo*

Key Laboratory for Intelligent Nano Materials and Devices of the Ministry of Education, and Institute of Nanoscience, State Key Laboratory of Mechanics and Control of Mechanical Structures, Nanjing University of Aeronautics and Astronautics, Nanjing, 210016, China.

Abstract

Evaporation induced electric potential in functional materials has been promoting the emergence of a new discipline, hydrovoltaics[1,2], but the phenomena have been widely ascribed to streaming potential related classic electrokinetic effects[3,4]. Here we show that evaporation in ambient environment can directly generate a sustainable voltage of up to 1 V with a current density of around 20 nA cm^{-2} from a porous carbon black film without contribution from streaming potential. Multi-electrode measurements confirm that the evaporating potential is generated mainly within the precursor ahead of the main capillary front. Detailed theoretical and experimental analyses indicate that the evaporating potential following the quadratic distribution arises from molecule evaporation induced carrier transfer in the precursor film. This new finding should lay a solid foundation for the emerging hydrovoltaics.

Harvesting energy from liquid evaporation has significant potential for green energy owing to the ubiquity of evaporation[1,2,5]. Evaporation has been widely used to drive microfluidic flow within porous films to generate electric power[3,4,6-14] mainly based on the classic streaming potential effect[15,16]. However, the interactions between materials and evaporating molecules have been rarely investigated. Here we show that ethanol evaporation from a porous carbon black (CB) film can directly generate a sustainable voltage of around 1 V, while streaming potential plays an ignorable role. We prove that evaporation of ethanol from the precursor film ahead of the main capillary region plays the core role in creating the electric potential in the CB film. This novel evaporating potential paves a new avenue for hydrovoltaic technology.

Our evaporation device is fabricated using an ethanol flame to deposit a thin CB film of size 1×1 cm^2 onto a ceramic substrate coated with equally-spaced carbon nanotube (CNT) ink electrodes E1~En (see **Methods** and Supplementary Figs. 1-2). When the bottom end of the film is inserted in bulk ethanol, a thin ethanol film will climb along the CB film through transpiration and capillary force (Fig. 1a). The thermal images taken by an infrared thermal camera in Fig. 1b show the rising process of the capillary front along a CB film with four electrodes (E1~E4) at a spacing of 3 mm. Real-time open circuit voltage variations are measured as well (Fig. 1c). The voltage produced in the process is in range of 0.2~1.5 V (Supplementary Fig. 3). As can be expected, controlling the ethanol evaporation state can manipulate the induced voltage (Supplementary Figs. 4 and 5), indicating a strong relevance of the electricity generation to ethanol evaporation rate. When evaporation is fully stopped (Supplementary Fig. 6) or the CB film is fully immersed in ethanol (Supplementary Fig. 7), the voltage decreases to around 0, indicating that possible chemical reactions can be excluded and the potential is induced by evaporation in our experiments[3,4]. Further investigations reveal that the thermoelectric potential of the CB film is on the millivolt level, which contributes little to the volt-level voltage in this system (Supplementary Fig. 8).

The streaming potential, a classic electrokinetic phenomenon in which an electric voltage can be generated when an electrolyte is driven through a narrow channel under a pressure gradient[15,16], plays an important role in previous experiments of evaporation induced electricity[3,4,6-14]. The dashed lines in Fig. 1c mark when the capillary front rise to E1, E2, and E3, respectively. It can be found that the voltage is merely generated between electrodes across the capillary front of the ethanol film,

which is in sharp contrast to water evaporation induced voltage which occurs in each neighbouring electrodes within the water capillary region and increases with increasing distance from the bulk water[4,12,13](Supplementary Fig. 9). This distinguished phenomenon means that no pronounced streaming potential occurs behind the capillary front. There may have two possible reasons: the ethanol moves up on the surface rather than streams through the porous CB film, or ethanol streaming through the CB film does not induce pronounced streaming potential.

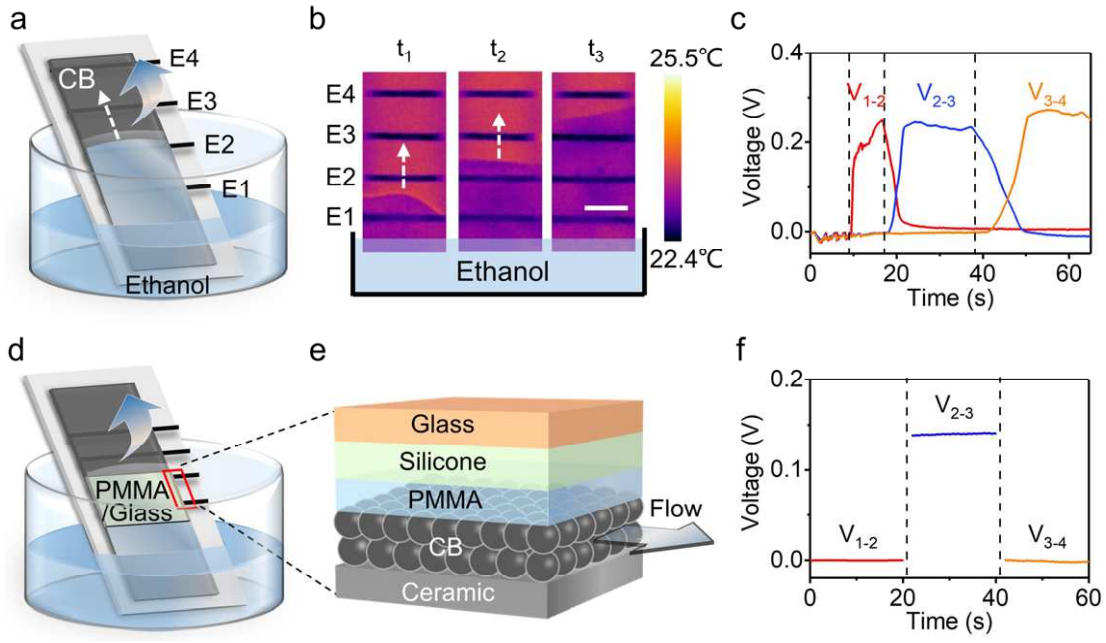

Figure 1. Evaporating potential in the CB film. **a**, Experimental set-up for electricity measurement of a four-electrode CB film during capillary process. The spacing between each two neighbouring electrodes is around 3 mm. The bottom end of the film is inserted in bulk ethanol. The dashed arrow indicates the capillary flow direction. **b**, Thermal images showing the rising capillary front of the CB film in **a**. Scale bar, 3 mm. **c**, Real-time voltage variations between each two neighbouring electrodes. The dashed lines mark when the capillary front rises to E1, E2, and E3, respectively. **d**, Experimental set-up for evaporation induced flow effect. The spacing between each two neighbouring electrodes is around 1 mm. The CB film between E1 and E2 is sealed with a PMMA layer to avoid evaporation and guarantee ethanol to flow within the porous CB only. The steady-state capillary front is maintained between E1 and E2. **e**, Schematic diagram illustrating the cross-section of the CB device between E1 and E2. **f**, Measured steady-state voltage distribution of the CB film in **d**.

The zeta potential of the CB in ethanol used in our experiments is measured to be around -1.69 mV, which is far weaker than that in DI water (-34.6 mV, Supplementary Fig. 10). This weak zeta potential means that the ethanol in our experiment should be difficult to supply ions to produce remarkable streaming potential[15]. To fully clarify the role of streaming potential, we design a specific four-electrode experiment to verify the contribution of the streaming effect as illustrated in Fig. 1d. The spacing between each two neighbouring electrodes is about 1 mm and the area between the bottom two electrodes (E1 and E2) is covered with a polymethylmethacrylate (PMMA) layer to avoid liquid evaporation while the rest part of the CB is exposed to air. The PMMA layer is further covered with silicone and glass for reinforcement to guarantee the ethanol to stream through the porous CB film in this section (Fig. 1e). The steady-state capillary front is maintained between E2 and E3 and the capillary film ahead of the PMMA layer is exposed to air to evaporate and drives the ethanol stream inside the porous CB underneath the PMMA layer. The measured ethanol streaming induced voltage signal is nearly zero between E1 and E2 (Fig. 1f), indicating that the contribution of streaming potential to the induced potential is ignorable. In contrast, evaporation driven water flow inside the porous carbon film beneath the PMMA layer can generate a voltage around 0.22 V (Supplementary Fig. 11).

Careful inspection shows that a thin precursor ethanol film[17-19] is always moving ahead of the main capillary front (Supplementary Fig. 12). We then use a tungsten steel needle to detect the voltage distribution in the precursor film, as illustrated in Fig. 2a. The steady-state capillary front is between E1 and E2 at a spacing of 1 cm in this case. The induced voltage between E1 and E2 ($V_{1\text{-}2}$) is measured to be around 1 V (Fig. 2b, purple line) with a short circuit current of around 20 nA (Supplementary Fig. 13). The inset (top left) in Fig. 2a shows the optical image of the needle with a distance d from the main capillary front. It is shown that no voltage V_d between the tip and E2 can be detected when d is larger than about 1.7 mm, while V_d increases with decreasing d below 1.7 mm, and reaches $V_{1\text{-}2}$ = 0.85 V at d approaching 0 (Fig. 2b). This result indicates that the evaporating potential is mainly induced by evaporating ethanol molecules within the precursor that is about 1.7 mm wide ahead of the main capillary film, while the streaming and evaporating processes in the main capillary region play little role.

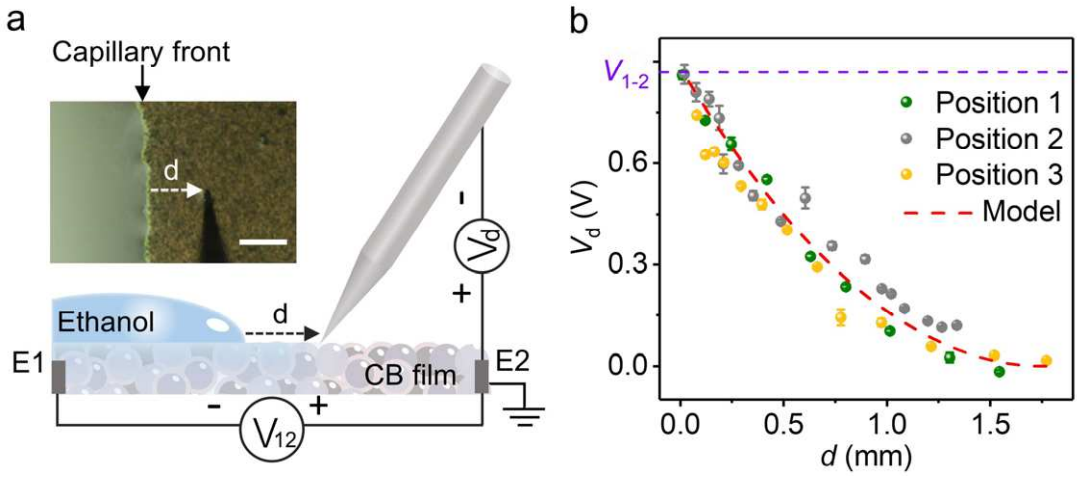

Figure 2. Potential distribution in the precursor film. a, Schematic illustration of the experimental set-up. Two CNT electrodes (E1 and E2) with a spacing of around 1 cm are deposited on the ceramic substrate underneath the CB film for voltage measurement ($V_{1\text{-}2}$). The tilt angle of the device is about 15º. Voltage distribution (V_d) in the precursor film ahead of the main capillary front is detected with a tungsten steel needle. The inset (top left) shows the optical image of the needle with a distance d from the main capillary front. Scale bar, 100 μm. **b**, Measured voltage distribution (V_d) in the precursor film. The circles denote the experimental data with bars indicating the standard deviation at three different positions. The red line indicates the modelling result. The purple line represents measured $V_{1\text{-}2}$.

To investigate the origin of the evaporating potential, we modify the surface functional groups of the CB film. Pristine CB materials are composed of loosely stacked graphene flakes with different oxygen-containing functional groups, such as C-O-C, C=O, and COOH groups, as confirmed by X-ray photoelectron spectroscopy (XPS) (Fig. 3a, top). We further modify the CB film with polyethyleneimine, turning the CB film into a N-doped state as shown in Fig. 3a (bottom) (atomic content of N is about 7.8%, Supplementary Fig. 14). Fourier transform infrared spectroscopy further validates the decrease of COOH groups and the existence of C=N bonds in the N-doped CB film (Supplementary Fig. 15)[20]. The saturated voltage of the pristine CB film is around 1.5 V while the measured voltage for the N-doped CB film is around -1.0 V (Fig. 3b).

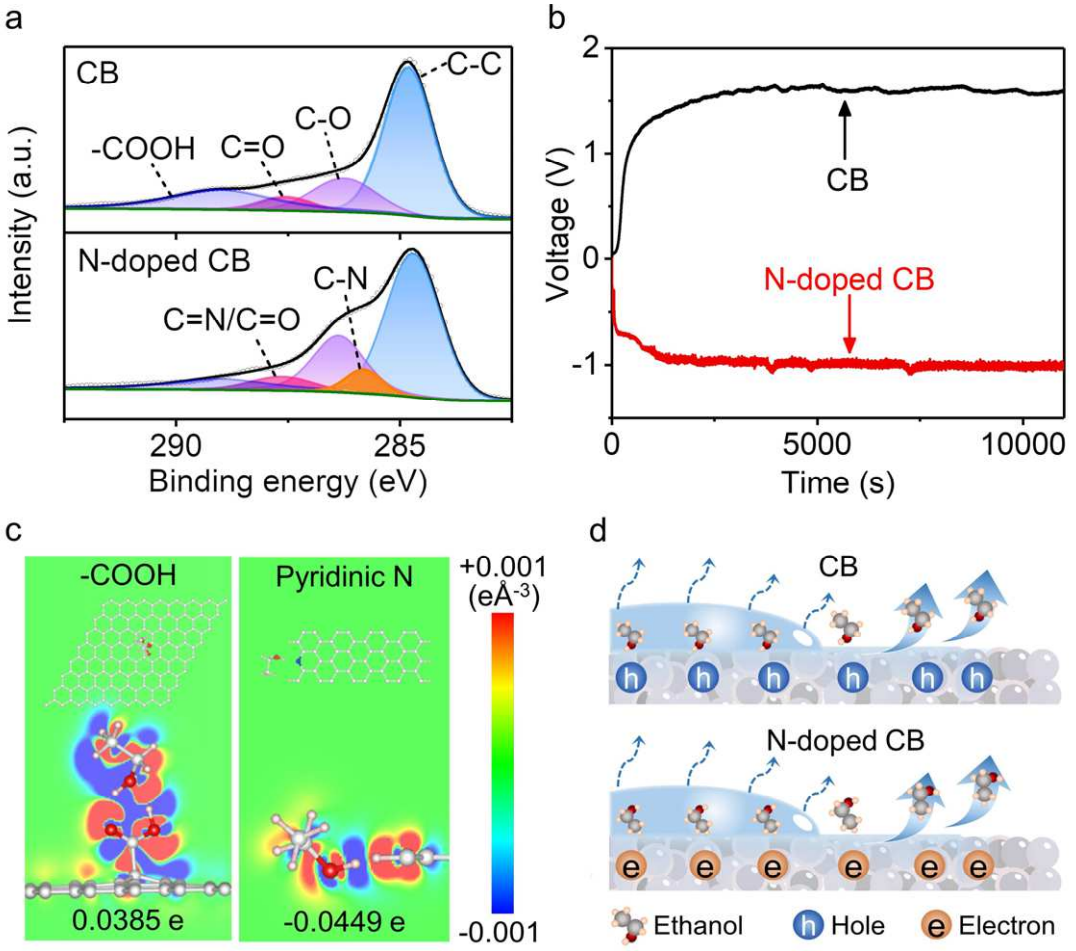

Figure 3. Mechanism for the evaporating potential. a, b, XPS spectrum (**a**) and measured voltage (**b**) for the pristine and N-doped CB film, respectively. **c**, Charge redistribution in the carboxyl graphene (left) and pyridinic-N-doped graphene (right) adsorbed with an ethanol molecule, respectively (red, gaining electron; blue, losing electron). The isosurface is set to 0.001 eÅ^{-3}. Electron redistribution in the carbon layer is labelled at the bottom. **d**, Schematic illustration of the evaporating potential as ethanol molecules evaporate from the pristine (top) and N-doped CB film (bottom), respectively.

To understand the effect of functional groups on the evaporating potential, we carry out first-principles calculations on the interaction between ethanol molecules and graphene flakes. When the graphene layer with carboxyl groups is adsorbed with an ethanol molecule, there is an electron accession of about 0.0385 e in the graphene layer (Fig. 3c, left; Supplementary Table 1). The accumulation of electrons on the upper surface of the graphene layer leads to the increase of hole concentration on the other side of graphene. In comparison, there is an electron depletion of about

0.0449 e in the pyridinic-N-doped graphene layer (Fig. 3c, right; Supplementary Table 1). Our molecular dynamics simulations further reveal the configuration transformation of an ethanol molecule during evaporation (Supplementary Fig. 16). For a CB film covered with a capillary ethanol film, ethanol molecules behind the main capillary front evaporate from the surface of the liquid film and do not interact with local CB directly, accordingly having no influence on charge distribution in the CB film. When ethanol molecules in the precursor film start to evaporate from the CB with carboxyl groups, accumulated electrons on the upper surface of the carbon layer return to the evaporating ethanol molecules, thus raising local hole concentration and electric potential in the CB film (Fig. 3d, top). Similarly, ethanol evaporation from N-doped CB induces a reversed potential difference (Fig. 3d, bottom). So, it is confident that the potential is induced by ethanol evaporation from the precursor, which can be termed as evaporating potential, a novel fundamental solid-liquid interaction distinct from the classic electrokinetic phenomena.

Following this mechanism, an equivalent capacitance-resistance model can be proposed to describe the distribution of evaporating potential in the precursor film (Supplementary Fig. 17). Ethanol molecules adsorbed on the CB film and accumulated holes in the precursor film can be simplified as a series of capacitors ($C_1 \sim C_n$). When ethanol molecules start to evaporate from the precursor film, capacitors ($C_1 \sim C_n$) will be more charged with higher potential than those underneath the ethanol film, driving a hole current from the precursor to the main capillary front. This model leads to a voltage distribution in the CB film as

$$V_d = \frac{v}{2\rho} \cdot q_0 \cdot R_{\mathrm{sq}} \cdot (L - d)^2 \tag{1}$$

where v is the average evaporation rate of ethanol in the precursor film, ρ is the density of ethanol, q_o is the discharging charge per volume, R_{sq} is the square resistance of the CB film, L is the length of the precursor film, and d is the distance from ΔR_m to the main capillary front (Supplementary Note 1). The detected voltage in the precursor film can be numerically fitted with a quadratic function (Fig. 2b) according to equation (1). In addition, the voltage-time curve of the CB device when the precursor film climbs across the two electrodes can be well fitted with quadratic functions based on equation (1) (Supplementary Fig. 18, Supplementary Note 2). Therefore, the proposed model is able to describe the evaporating potential in the precursor efficiently.

Discussion

We find that the evaporating potential is sensitive to gas flow and ethanol vapor. Using these features, we construct a self-powered sensor to monitor gas flow or ethanol vapor in the ambient environment as shown in Fig. 4a, where a CB device acts as the gate of a transistor, controlling the illumination of an LED powered by a 3 V battery. When the gas flow at a rate of 1 m s^{-1} blows the CB film, ethanol rapidly evaporates from the CB and the precursor film is suppressed between the two electrodes, giving rise to an increased current and illuminating the LED (Fig. 4b). When the concentration of ethanol vapor increases in ambient environment, the current of the CB device decreases, leading the LED to get dark (Fig. 4c).

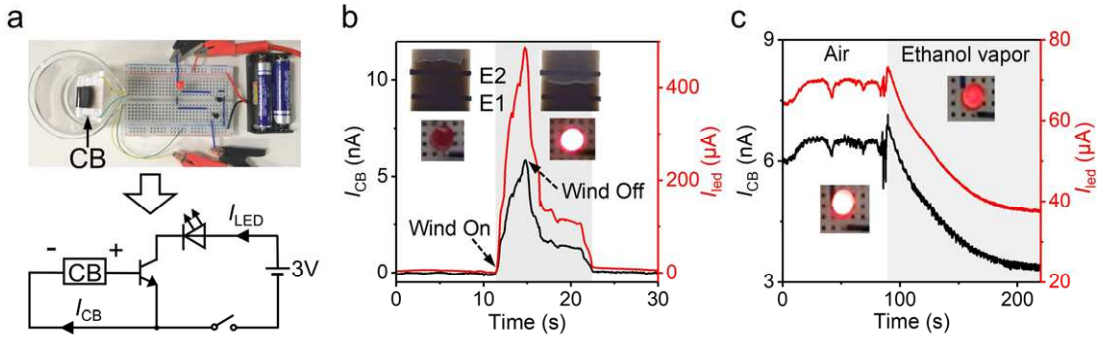

Figure 4. Demo of the evaporating potential. a, Evaporating potential based CB sensor. The self-powered CB device acts as the gate of a transistor to control the illumination of an LED, which is sensitive to gas flow and ethanol vapor. The equivalent circuit is illustrated at the bottom. **b**, Response of I_{CB} and I_{led} to gas flow. The main capillary front is ahead of E2 without gas flow. Once the flow at a rate of 1 m s^{-1} blows the CB film, the main capillary front is maintained between E1 and E2 and the transistor turns on, illuminating the LED. **c**, Response of I_{CB} and I_{led} to ethanol vapor. The LED gets dark as the concentration of ethanol vapor increases in ambient environment.

The output performance of a CB device of size 1×1 cm^2 is measured by connecting external loads with different resistances. As the load resistance increases from 10 kΩ to 10 GΩ, the output voltage rises from around 0 to ~1.8 V while the current drops from ~21 nA to around 0 (Supplementary Fig. 19a). The CB generator has a maximum power density of ~90 μW/m^2 at external resistance of 80 MΩ (Supplementary Fig. 19b). The induced V_{oc} and I_{sc} can be scaled by connecting the CB devices in series and in parallel, respectively (Supplementary Fig. 20). Moreover,

the produced electricity can be stored in capacitors (Supplementary Fig. 21a), which can further power a liquid crystal display (Supplementary Fig. 21b).

We have revealed a novel physical effect of evaporating potential induced by direct ethanol evaporation in the precursor on a CB film. In contrast to all the previous investigations for evaporation induced potential, the evaporating potential is free from streaming potential and originates from charge transfer at the solid-liquid interfaces. This work provides a new perspective on the interactions between solid and evaporating molecules, demonstrating a promising approach for green energy and self-powered sensors, thus, laying a solid foundation for the emerging hydrovoltaics.

Methods

Device fabrication. As shown in Supplementary Fig. 1, the ceramic plate (3×5 cm^2) was ultrasonically cleaned (Supplementary Fig. 1-I) and printed with CNT ink to form electrodes with width of around 1 mm (Supplementary Fig. 1-II). Then, a uniform CB film was grown on the ceramic substrate across the electrodes over an ethanol flame (Supplementary Fig. 1-III), which was subsequently annealed at 400 ℃ in air for 2 h (Supplementary Fig. 1-IV). Afterwards, the device was wired and the exposed electrodes were carefully covered by silicone (Supplementary Fig. 1-V). Finally, the CB device was laid in a beaker containing ethanol for electricity measurement (Supplementary Fig. 1-VI).

Nitrogenous functional groups doping. The CB film was immersed in an aqueous polyethyleneimine solution (0.1 wt%) and then kept at a temperature of 80 °C for 4h in a water bath. After being thoroughly washed with DI water, the CB film was further immersed in an aqueous glutaraldehyde solution (0.1 wt%) and kept at a temperature of 80 °C for 4h in a water bath. Finally, the CB film was thoroughly washed with DI water and ethanol to remove residuals and the N-doped CB film was obtained.

Characterizations and measurements. The morphology and structure of the CB device were investigated by scanning electron microscope (ZEISS Sigma 300) and transmission electron microscopy (JEOL JEM2100F). The thermal images of the CB film were taken by an infrared thermal camera (Fotric 226s). The functional groups of CB were characterized by X-ray

photoelectron spectrometer (EscaLab 250Xi) and Fourier-transform infrared spectrometer (Nicolet iS5). The temperature and humidity were measured by a temperature and humidity meter (TH22R-EX). The real-time open-circuit voltage and short-circuit current were measured by a Keithley DMM6500 multimeter.

First-principles calculations. First-principles calculations were performed within the framework of density-functional theory as encoded in Vienna Ab-initio Simulation Package code[21-23]. The projector-augmented wave method was employed for the core region based on generalized gradient approximation (GGA)[24]. All the results were calculated with the advanced vdW-DF method[25] for dispersion correction and the optB86b-vdW functional for describing the exchange functional. The kinetic energy cutoff of the plane-wave expansion was set to be 500 eV. The atomic geometries were fully relaxed with conjugate gradient method until the force on each atom is less than 0.01 eV/Å and a total energy convergence of 10^{-5} eV. A vacuum space of 15 Å was set to isolate neighbouring periodic images.

To elucidate the mechanism, two types of theoretical models based on DFT calculations were built in this work, ethanol molecules adsorbed on the graphene layer and at the edge of the armchair graphene nanoribbon (AGNR). To study the ethanol molecule adsorption on the surface of (functional) graphene, ethanol molecules adsorbed on an 8×8 supercell of graphene were compared without/with functional groups. The Brillouin zone was sampled with 3×3×1 grid in the calculations. For ethanol molecules adsorbed at the edge of the (functional) graphene nanoribbon, ethanol molecules adsorbed at the edge of a periodic H-passivated 13-AGNR were compared without/with functional groups. The k-mesh was set to 1×32×1. For each type of adsorption, various adsorption positions of the ethanol molecule were taken into consideration while their adsorption energies and the charge redistributions were compared.

The adsorption energy (E_{ad}) of the ethanol molecule was calculated as

$$E_{\mathrm{ad}} = E_{\mathrm{FG+E}} - E_{\mathrm{FG}} - E_{\mathrm{E}} \quad (2)$$

where E_{FG+E}, E_{FG} and E_E are the energy of the whole adsorption system, graphene without/with functional groups and the ethanol molecule, respectively.

The charge redistribution was defined as

$$\Delta\rho = \rho_{\mathrm{FG+E}} - \rho_{\mathrm{FG}} - \rho_{\mathrm{E}} \quad (3)$$

where the ρ_{FG+E}, ρ_{FG}, and ρ_E denotes the charge distribution of the whole adsorption system,

graphene without/with functional groups and the ethanol molecule, respectively. To give a direct comparison on numerical value for electron transfer, Bader analysis was used to calculate the charge transfer in atoms.

Molecular-dynamics simulation. A graphene sheet oxidized by carboxyl groups, with a size of 6×7 nm^2, was constructed to mimic the surface of the carbon black substrate. The overall ratio of carbon and oxygen is about 4.5, similar to that in our experiments. The atoms are precharged according to the results of first-principles calculations. An ethanol molecule was initially put near the substrate, leaving a vacuum layer with a thickness of about 10 nm. Periodic boundary conditions were applied in all directions of the system. All MD simulations were carried out in the NVT ensemble with the software NAMD[26]. The Langevin dynamics was used to control the temperature at 300 K[27]. The time step was set to 2 fs. Parameters for both the oxidized graphene and the ethanol molecule were obtained by using SWISS-MODEL[28].

References

1 Zhang, Z. *et al*. Emerging hydrovoltaic technology. *Nat. Nanotech.* **13**, 1109–1119 (2018).

2 Yin, J., Zhou, J., Fang, S., & Guo, W. Hydrovoltaic energy on the way. *Joule* **4**, 1852–1855 (2020).

3 Liu, Z. *et al.* Surface-energy generator of single-walled carbon nanotubes and usage in a self-powered system. *Adv. Mater.* **22**, 999–1003 (2010).

4 Xue, G. *et al.* Water-evaporation-induced electricity with nanostructured carbon materials. *Nat. Nanotech.* **12**, 317–321 (2017).

5 Cavusoglu, A.-H., Chen, X., Gentine, P. & Sahin, O. Potential for natural evaporation as a reliable renewable energy resource. *Nat. Commun.* **8**, 617 (2017).

6 Li, J. *et al.* Surface functional modification boosts the output of an evaporation-driven water flow nanogenerator. *Nano Energy* **58**, 797–802 (2019).

7 Shao, C. *et al*. Large-Scale Production of Flexible, High-voltage hydroelectric films based on solid oxides. *ACS Appl. Mater. Interfaces* **11**, 30927–30935 (2019).

8 Sun, J. *et al.* Electricity generation from a Ni-Al layered double hydroxide-based flexible generator driven by natural water evaporation. *Nano Energy* **57**, 269–278 (2019).

9 Zhang, G. *et al.* Harvesting environment energy from water-evaporation over free-standing graphene oxide sponges. *Carbon* **148**, 1–8 (2019).

10 Zhou, X. *et al.* Harvesting electricity from water evaporation through microchannels of natural wood. *ACS Appl. Mater. Interfaces* **12**, 11232–11239 (2020).

11 Qin, Y. *et al.* Constant electricity generation in nanostructured silicon by evaporation-driven water flow. *Angew. Chemie. Int. Ed*. **132**, 2–9 (2020).

12 Li, L. *et al.* Sustainable and flexible hydrovoltaic power generator for wearable sensing electronics. *Nano energy* **72**, 104663 (2020).

13 Ma, Q. et al. Rational design of MOF-based hybrid nanomaterials for directly harvesting

electric energy from water evaporation. *Adv. Mater.* **2003720**, 1–6 (2020).
14 J Bae, J., Yun, T. G., Suh, B. L., Kim, J. & Kim, I. D. Self-operating transpiration-driven electrokinetic power generator with an artificial hydrological cycle. *Energy Environ. Sci.* **13**, 527–534 (2020).
15 Delgado, Á. V. *et al*. Measurement and interpretation of electrokinetic phenomena. *J. Colloid Interface Sci.* **309**, 194–224 (2007).
16 Van der Heyden, F. H. J. *et al.* Power generation by pressure-driven transport of ions in nanofluidic channels. *Nano Lett.* **7**, 1022–1025 (2007).
17 Balankin, A. S., Paredes, R. G., Susarrey, O., Morales, D. & Vacio, F. C. Kinetic roughening and pinning of two coupled interfaces in disordered media. *Phys. Rev. Lett.* **96**, 1–4 (2006).
18 Popescu, M. N., Oshanin, G., Dietrich, S. & Cazabat, A. M. Precursor films in wetting phenomena. *J. Phys. Condens. Matter* **24**, 243102 (2012).
19 Chibbaro, S. *et al.* Evidence of thin-film precursors formation in hydrokinetic and atomistic simulations of nano-channel capillary filling. *Epl* **84**, 1–11 (2008).
20 Pan, N. *et al*. A Schiff base/quaternary ammonium salt bifunctional graphene oxide as an efficient adsorbent for removal of Th(IV)/U(VI). *J. Colloid Interface Sci.* **508**, 303–312 (2017).
21 Kresse, G. & Hafner, J. Ab initio molecular dynamics for liquid metals. Phys. *Rev. B* **47**, 558–561 (1993).
22 Kresse, G. & Furthmüller, J. Self-interaction correction to density functional approximation for many electron systems. *Phys. Rev. B* **54**, 11169 (1996).
23 Kresse, G. & Joubert, D. From ultrasoft pseudopotentials to the projector augmented-wave method. *Phys. Rev. B* **59**, 1758 (1999).
24 Perdew, J. P., Burke, K. & Ernzerhof, M. Generalized gradient approximation made simple. *Phys. Rev. Lett.* **77**, 3865 (1996).
25 Klimeš, J., Bowler, D. R. & Michaelides, A. Chemical accuracy for the van der Waals density functional. *J. Phys.: Cond. Matt.* **22**, 022201 (2009).
26 Phillips, J. C. *et al*. Scalable molecular dynamics with NAMD. *J. Comput. Chem.* **26**, 1781–1802 (2005).
27 Feller, S. E., Zhang, Y., Pastor, R. W. & Brooks, B. R. Constant pressure molecular dynamics simulation: The Langevin piston method. *J. Chem. Phys.* **103**, 4613–4621 (1995).
28 Schwede, T., Kopp, J., Guex, N. & Peitsch, M. C. SWISS-MODEL: An automated protein homology-modeling server. *Nucleic Acids Res.* **31**, 3381–3385 (2003).

Acknowledgements

This work was supported by NSF (51535005), the Fundamental Research Funds for the Central Universities (NJ2020003, NJ2019002, NP2019301, NC2018001), A Project Funded by the Priority Academic Program Development of Jiangsu Higher Education Institutions. Y.X. is supported by NSF of China (51802153), the National Postdoctoral Program for Innovative Talent of China (BX20180141) and the Postdoctoral Science Foundation of China and Jiangsu Province (2018M642247, 2018K163C).

Author Contributions

W.G. and S.F. conceived the idea of the project and designed the experiments. S.F. and J.L.

performed the experiments. Y.X. performed the DFT calculations. C.S. conducted the molecular dynamics simulations. W.G. supervised the research. All authors contributed to the analysis, discussion and writing of the manuscript.

Figures

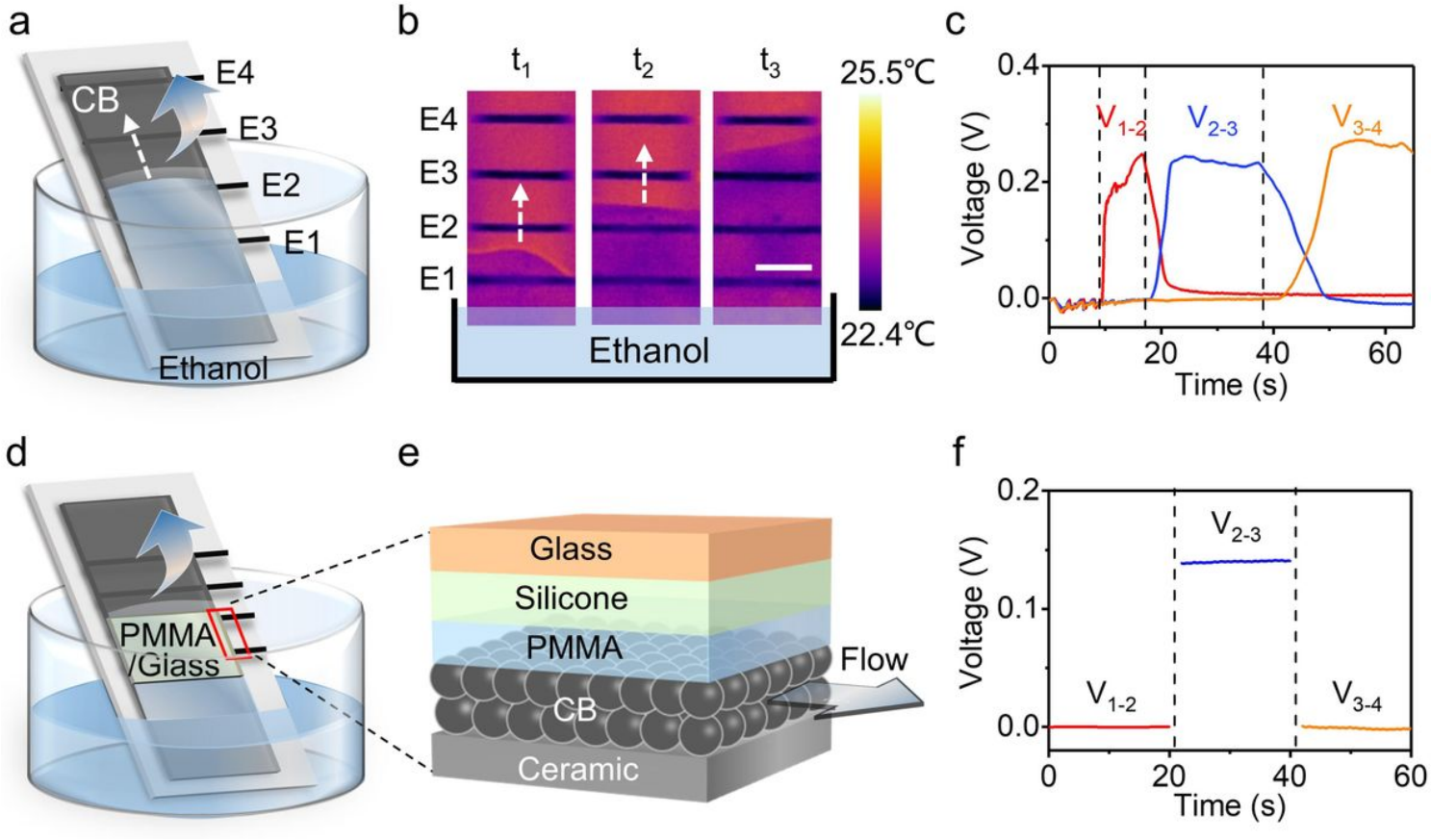

Figure 1

Evaporating potential in the CB film. a, Experimental set-up for electricity measurement of a four-electrode CB film during capillary process. The spacing between each two neighbouring electrodes is around 3 mm. The bottom end of the film is inserted in bulk ethanol. The dashed arrow indicates the capillary flow direction. b, Thermal images showing the rising capillary front of the CB film in a. Scale bar, 3 mm. c, Real-time voltage variations between each two neighbouring electrodes. The dashed lines mark when the capillary front rises to E1, E2, and E3, respectively. d, Experimental set-up for evaporation induced flow effect. The spacing between each two neighbouring electrodes is around 1 mm. The CB film between E1 and E2 is sealed with a PMMA layer to avoid evaporation and guarantee ethanol to flow within the porous CB only. The steady-state capillary front is maintained between E1 and E2. e, Schematic diagram illustrating the cross-section of the CB device between E1 and E2. f, Measured steady-state voltage distribution of the CB film in d.

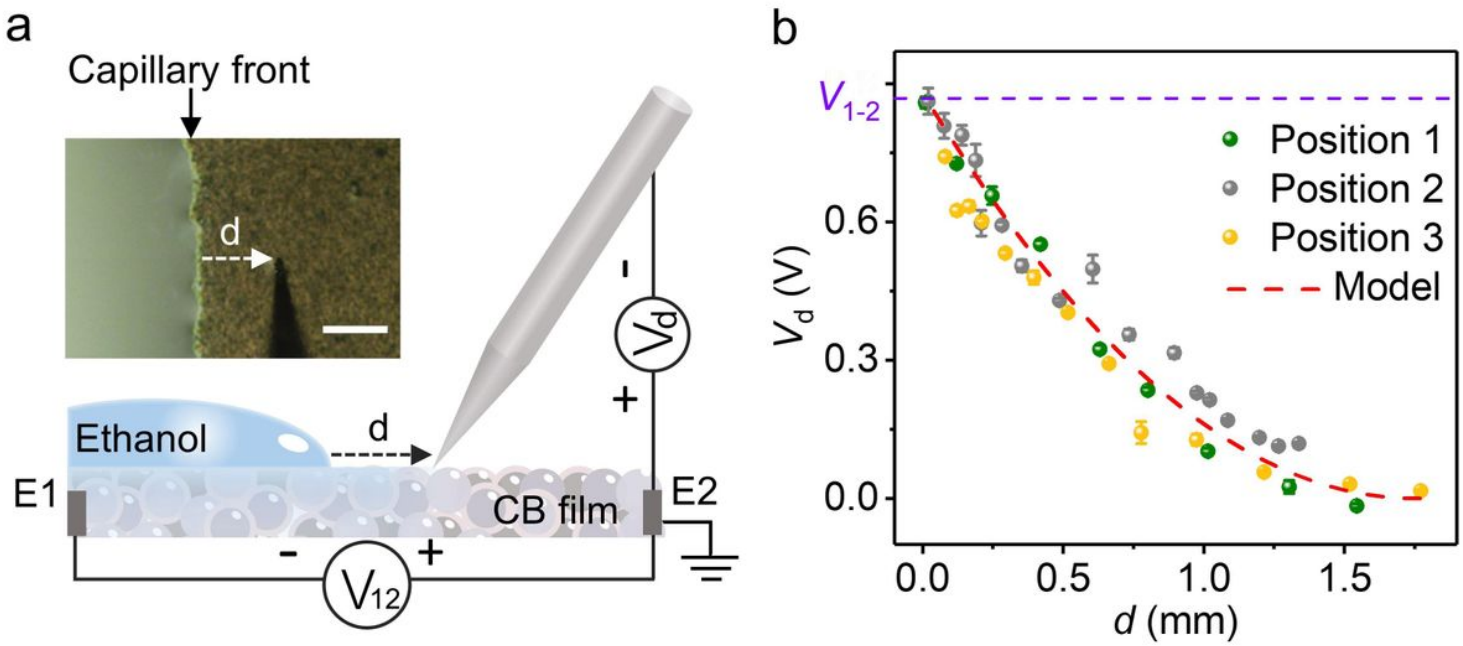

Figure 2

Potential distribution in the precursor film. a, Schematic illustration of the experimental set-up. Two CNT electrodes (E1 and E2) with a spacing of around 1 cm are deposited on the ceramic substrate underneath the CB film for voltage measurement (V1-2). The tilt angle of the device is about 15º. Voltage distribution (Vd) in the precursor film ahead of the main capillary front is detected with a tungsten steel needle. The inset (top left) shows the optical image of the needle with a distance d from the main capillary front. Scale bar, 100 μm. b, Measured voltage distribution (Vd) in the precursor film. The circles denote the experimental data with bars indicating the standard deviation at three different positions. The red line indicates the modelling result. The purple line represents measured V1-2.

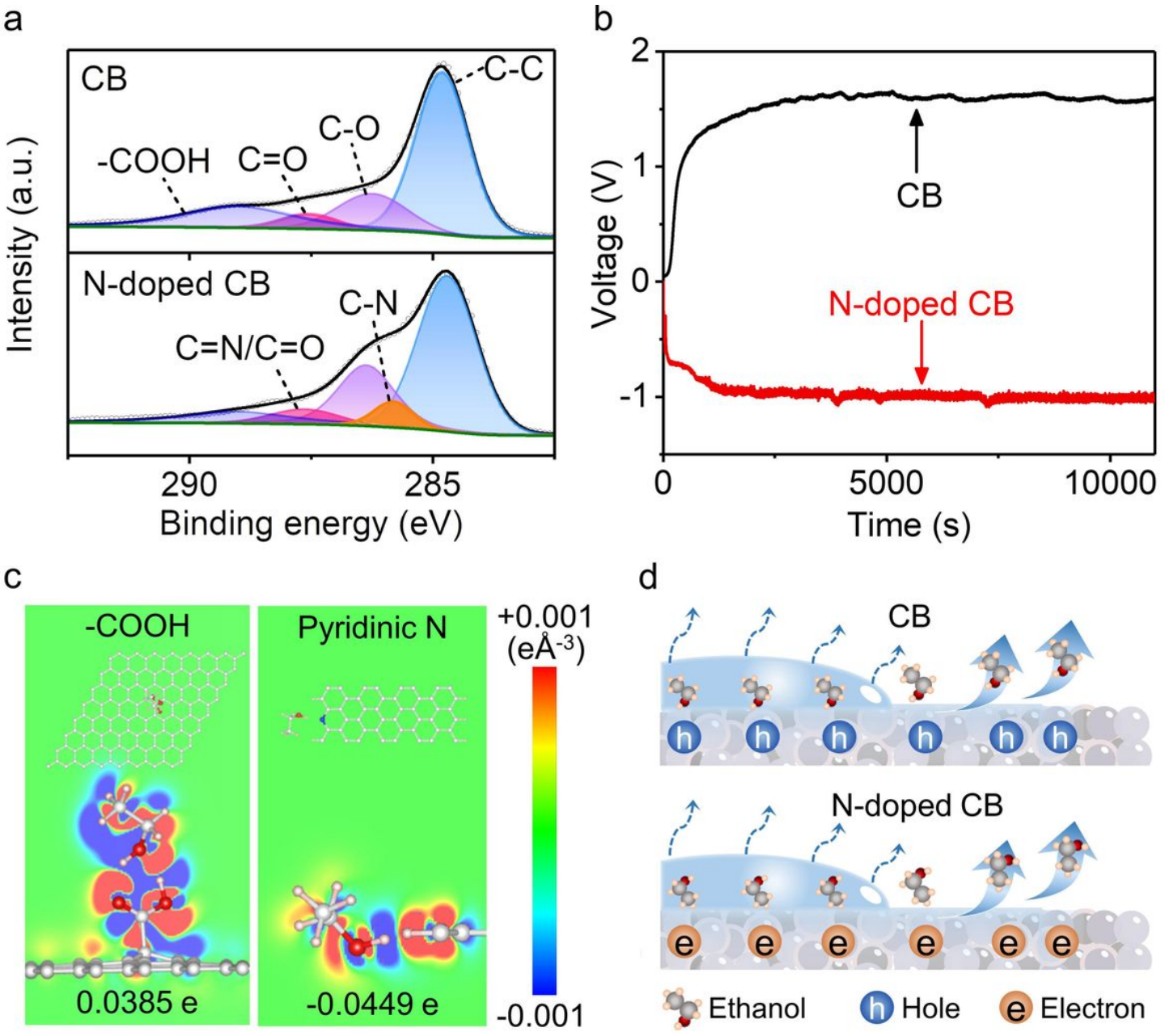

Figure 3

Mechanism for the evaporating potential. a, b, XPS spectrum (a) and measured voltage (b) for the pristine and N-doped CB film, respectively. c, Charge redistribution in the carboxyl graphene (left) and pyridinic-N-doped graphene (right) adsorbed with an ethanol molecule, respectively (red, gaining electron; blue, losing electron). The isosurface is set to 0.001 eÅ−3. Electron redistribution in the carbon layer is labelled at the bottom. d, Schematic illustration of the evaporating potential as ethanol molecules evaporate from the pristine (top) and N-doped CB film (bottom), respectively.

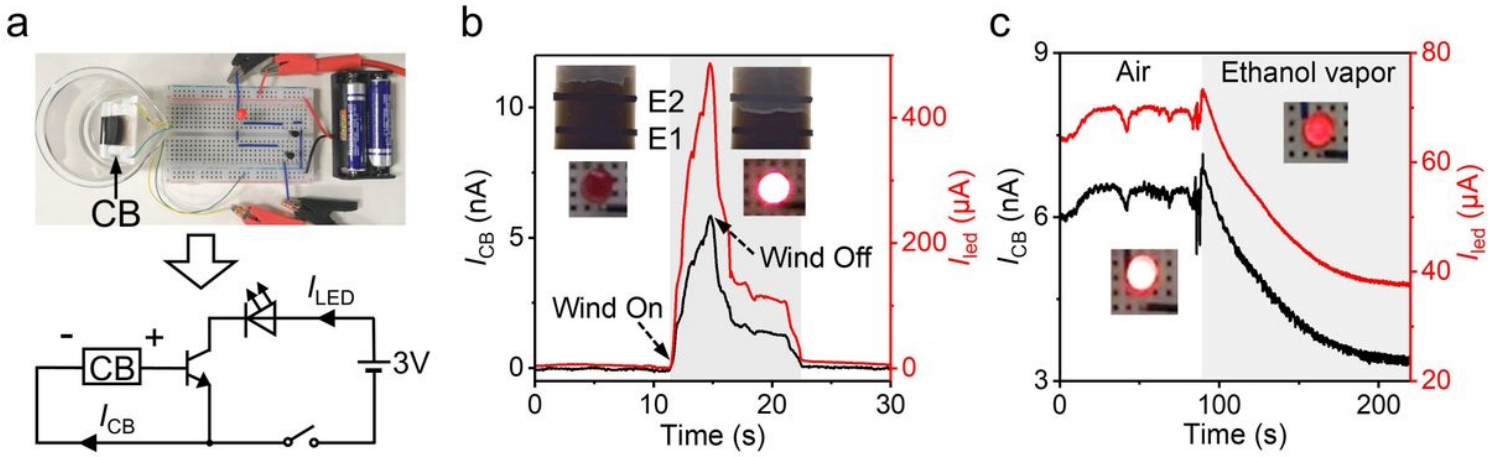

Figure 4

Demo of the evaporating potential. a, Evaporating potential based CB sensor. The self powered CB device acts as the gate of a transistor to control the illumination of an LED, which is sensitive to gas flow and ethanol vapor. The equivalent circuit is illustrated at the bottom. b, Response of ICB and Iled to gas flow. The main capillary front is ahead of E2 without gas flow. Once the flow at a rate of 1 m s-1 blows the CB film, the main capillary front is maintained between E1 and E2 and the transistor turns on, illuminating the LED. c, Response of ICB and Iled to ethanol vapor. The LED gets dark as the concentration of ethanol vapor increases in ambient environment.

Supplementary Files

This is a list of supplementary files associated with this preprint. Click to download.

- Supplementaryinformation.pdf